Electron microscopy of cytochrome *c* oxidase-containing proteoliposomes: imaging analysis of protein orientation and monomer–dimer behaviour

Mariana TIHOVA,* Brenda TATTRIE and Peter NICHOLLS†
Department of Biological Sciences, Brock University, St. Catharines, Ontario L2S 3A1, Canada

1. Cytochrome *c* oxidase-containing vesicles were prepared by cholate dialysis using bovine heart cytochrome *c* oxidase with egg and dioleoylphosphatidylcholine/dioleoylphosphatidylethanolamines (1:1, w/w) at two ratios of phospholipid to protein (25 mg/mg and 10 mg/mg). With each mixture, one or two (FII, FIII) fractions with mostly outward-facing cytochrome aa_3 were separated from a fraction (FI) containing mostly inward-facing enzyme and protein-free liposomes by DEAE-Sephacel chromatography. 2. FII and FIII fractions from egg phospholipid mixtures had 60–80% outward-facing enzyme; FII and FIII fractions from dioleoyl phospholipids showed 50–70% outward-facing enzyme. Egg and dioleoyl phospholipid mixtures maintained good respiratory control ratios (8–13) only at the higher lipid/protein ratios. 3. Platinum/carbon replicas of freeze–fractured vesicle surfaces were subjected to image analysis. The results showed two types of membrane projection with average heights of 7.5 nm and 3.5 nm from the fracture plane. The former were more numerous on the convex faces. Calculated areas of the projections indicated the probable presence of both enzyme dimers and higher aggregates. Oxidase dimers may have membrane areas of 70–80 nm² at the high (7.5 nm) side and 40–50 nm² on the low (3.5 nm) side. 4. Proteoliposomes prepared with enzyme depleted of subunit III contained predominantly much smaller projecting areas. These probably represent monomers with high side areas of 35–40 nm² and low side areas of 20–25 nm². Electron microscopy thus directly confirms the predicted change of aggregation state resulting from subunit depletion. 5. The results are compared with those from two-dimensional crystals. Assuming that the high and low projections are two sides of one family of transmembrane molecules, a total length of 11 nm matches 11–12 nm lengths obtained by crystallography. Our membrane areas match the areas obtained in earlier 'crystal' studies better than the small areas obtained recently by electron cryomicroscopy.

INTRODUCTION

Eukaryotic cytochrome *c* oxidase is a multisubunit enzyme spanning the inner mitochondrial (cristal) membrane (Capaldi et al., 1987; Saraste, 1990; Cooper et al., 1991). Where is this rather large complex located in that membrane? Observations on freeze–fractured mitochondria (rat heart muscle) have shown a particulate structure for the cristae with closely packed particles ranging from 3 to 10 nm in diameter and an intermembrane distance of 26 nm within the cristae. The matrix surface of the cristal membrane is fairly smooth with only a few particles raised somewhat above the average surface level (Sjöstrand, 1990).

Cytochrome oxidase isolated in the form of two-dimensional (quasi)crystals is sufficiently pure to allow size and shape determination. These 'crystals' fall into two classes depending on differences in packing arrangements. Triton-derived specimens (Henderson et al., 1977) form collapsed vesicles with the dimeric enzyme inserted across the bilayers. Specimens obtained with deoxycholate (Fuller et al., 1979) form detergent-rich sheets without membrane bilayers. Three-dimensional analysis of the latter revealed monomers with two arms extending slightly above the membrane surface on the matrix (M) side and a single large domain on the cytoplasmic (C) side extending several nm from the surface. Valpuesta et al. (1990) have recently obtained a higher-resolution structure in ice-embedded vesicle crystals which showed a very compact hydrophobic region with no detectable branches.

Cytochrome oxidase-reconstituted vesicles (COV) have provided substantial information concerning enzyme function and properties, both in this laboratory (Nicholls and Shaughnessy, 1985; Nicholls et al., 1988a,b, 1990; Wrigglesworth et al., 1990; Nicholls, 1990) and elsewhere (Krab and Wikström, 1978; Moroney et al., 1984; Papa et al., 1987; Brunori et al., 1987; Gregory and Ferguson-Miller, 1989; Wilson and Prochaska, 1990). Such COV have also been used to study lipid–protein interactions (Longmuir et al., 1977; Falk and Karlsson, 1979; Costello and Frey, 1982; Robinson, 1982; Rigell et al., 1985; Rietveld et al., 1987; Fajer et al., 1989; Powell et al., 1990) and the lipid requirements for reconstituted enzyme orientation, activity and respiratory control (Vik and Capaldi, 1977; Casey et al., 1982; Madden et al., 1984; Zhang et al., 1985). Respiratory control is obtained when the oxidase is reconstituted with mixtures of phospholipids but usually not with vesicles composed of a single lipid species (Racker, 1972). Reconstitution with either dioleoylphosphatidylcholine (DOPC) or dioleoylphosphatidylethanolamine (DOPE) alone gave low enzyme activity (Madden et al., 1983), but with mixtures of the two lipids tightly controlled proteoliposomes have been obtained.

In the present work ultrastructural investigations of COV were combined with kinetic and spectroscopic measurements to study the effects of phospholipid composition upon enzyme activity, respiratory control ratio and orientation within the bilayer. With image analysis it has also been possible to analyse the pattern of protein insertion into the membrane, the distribution of the inlaid enzyme among monomers, dimers and oligomers, and the sizes of individual and average incorporated enzyme forms, to

Abbreviations used: DOPC, dioleoylphosphatidylcholine; DOPE, dioleoylphosphatidylethanolamine; eggPC, egg phosphatidylcholine; eggPE, egg phosphatidylethanolamine; COV, cytochrome oxidase-containing vesicles (proteoliposomes); SUIII-depleted, subunit III-depleted; Pt/C, platinum/carbon; L/P ratio, phospholipid to protein ratio.

* Present address: Department of Psychology, Life Sciences Centre, Dalhousie University, Halifax, Nova Scotia B3H 4J1, Canada.
† To whom correspondence should be addressed.

compare with the results from two-dimensional crystal analysis. Preliminary versions of this work have been presented by Tihova et al. (1991, 1992) and Nicholls et al. (1992).

MATERIALS AND METHODS

Preparation of enzyme

Cytochrome *c* oxidase was isolated from bovine heart essentially as described by Kuboyama et al. (1972), with Tween 80 substituting for Emasol as the final detergent, as described previously (Nicholls and Hildebrandt, 1978). It was stored at −80 °C in a buffer containing 100 mM sodium phosphate, pH 7.4, and 0.25 % Tween 80 at a concentration of 300–500 μM cytochrome aa_3 (0.6–1.0 mM haem *a* and between 60 and 100 mg of protein/ml). Storage in lauryl maltoside did not change the properties of the enzyme when thawed and diluted (a 'resting' enzyme Soret peak persisted at 418–420 nm).

Subunit III-depleted (SUIII-depleted) enzyme

The enzyme was depleted of subunit III as well as some of the smaller subunits by a variant of the method of Hill and Robinson (1986). Isolated 'resting' enzyme was incubated in 20 mM Tris/HCl buffer, pH 7.8, containing 0.5 % lauryl maltoside, 1 mM EDTA and 1 M NaCl, for 24 h at 25 °C, at a detergent/protein ratio of 8.4 (w/w). The incubation mixture was desalted by passage through a Sephadex G-25 column which was equilibrated and eluted with 20 mM Tris/HCl, pH 7.8, containing 0.1 % lauryl maltoside. The aa_3-containing fractions from this column were loaded on to a DEAE-Sephacel column previously equilibrated with 20 mM Tris/HCl buffer, pH 7.8, containing 0.1 % lauryl maltoside, and the column was washed with 20 mM Tris/HCl, pH 7.8, containing 0.8 % lauryl maltoside, to remove released subunit III (together with some smaller subunits). The SUIII-depleted enzyme was then eluted with 20 mM Tris/HCl buffer, pH 7.8, containing 0.3 M KCl and 2 % sodium cholate. SDS slab gel electrophoretic analysis showed that subunit III had indeed been removed (> 90 %) from these samples.

Lipids and other reagents

Phosphatidylcholine from egg yolk (eggPC) and phosphatidylethanolamine from egg yolk (eggPE) were obtained from Lipid Products as grade 1 in chloroform/methanol. Dioleoyl-L-α-phosphatidylcholine (DOPC) and dioleoyl-L-α-phosphatidylethanolamine (DOPE) were obtained in dry form from Avanti Polar Lipids (Alabaster, AL, U.S.A.). Cytochrome *c* (type VI) from horse heart was from Sigma Biochemicals (St. Louis, MO, U.S.A.). Other reagents were of analytical or similar quality wherever obtainable.

Preparation and fractionation of vesicles

Cytochrome *c* oxidase was incorporated into phosphatidylcholine/phosphatidylethanolamine (1 : 1, w : w) mixtures at different phospholipid to protein ratios using the two phospholipid mixtures: eggPC plus eggPE and DOPC plus DOPE. In each case 13–20 mg/ml lipid mixture was dispersed in 100 mM potassium Hepes buffer containing 1.5 % sodium cholate, pH 7.4. Protein-free liposomes were prepared by sonication for 7 min using a Heat Systems Ultrasonics W-375 sonicator in the pulsed mode at 30 % duty cycle and power 3, with the sample on ice and under a stream of nitrogen. The sample was centrifuged at 20000 ***g*** for 10 min and any pellet was discarded. Cytochrome oxidase (approx. 400 μM, 80 mg/ml stock solution in 100 mM sodium phosphate, pH 7.4, containing 0.25 % Tween 80) was added at a final concentration of 4–10 μM (0.8–2.0 mg/ml) to obtain phospholipid to protein ratios (L/P) equal to 25 mg/mg and 10 mg/mg, respectively. After being mixed, the samples were dialysed against 100 vol. of 100 mM Hepes buffer, pH 7.4, for 4 h and then against three changes of 10 mM Hepes, pH 7.4, containing 40 mM KCl and 50 mM sucrose for 2 days (a total of 800 vol.). Residual free cholate and Tween 80 after dialysis are negligible.

Cytochrome oxidase (aa_3) is non-randomly incorporated into COV (Madden et al., 1983; Scotto and Zakim, 1985; Wrigglesworth et al., 1987). Vesicles with outward-facing (and some inward-facing) cytochrome aa_3 were separated from the protein-free liposomes and/or the population containing mainly inward-oriented enzyme molecules by DEAE-Sephacel chromatography. The column (1.5 cm × 22 cm) was previously equilibrated with 25 mM potassium phosphate buffer, pH 7.4. A set of 1 ml samples was collected at a flow rate of 0.8 ml/min employing stepwise elution with increasing concentrations of potassium phosphate buffer, pH 7.4. The eluted fractions (FI, FII and FIII) were then concentrated to final volumes between 0.6 ml and 1.0 ml using Amicon Centriprep-10 ultrafilters. Table 1 summarizes their L/P ratios and other characteristics.

Electron microscopy

Vesicle samples (0.1–0.2 ml) were rapidly spray-frozen from 0 °C without a cryoprotectant on a standard Balzers Spray Freezing Unit type 12024 (Rand et al., 1985). Freeze–fracturing was carried out with a Balzers 400T apparatus (Hudson, NY, U.S.A.), using quartz-crystal-monitored Pt/C shadowing (45°, Pt thickness 1.5–2.0 nm) and forming replicas at −150 °C and 5×10^{-6} Pa. These were examined with a Philips 300 electron microscope.

Image analysis and size calculation

The size distribution of the enzyme particles and their contribution to the total vesicle area were determined using a Microcomputer Imaging System (MCID) from Imaging Research Inc., Brock University, St. Catharines, Ont. L2S 3A1, Canada. This comprised an appropriate video camera mounted above the electron microscope negative, an OS/2-based 80386 computer and the necessary commercial software (MCID with the Imaging Research Inc. package 'BRS' as the main program). The individual particle areas are measured semiautomatically by first outlining them and then measuring the outlined area. The same number of particles was measured for each experiment. The size of each projection includes a component from the platinum particles involved which cover the surface concerned. A correction for the values obtained directly was therefore made by applying eqn. (1):

$$A_{corr.} = \pi\left[\sqrt{\left(\frac{A_{meas.}}{\pi}\right)} - d\right]^2 \quad (1)$$

where $A_{corr.}$ = the corrected area, $A_{meas.}$ = the original measured area, and d = the apparent diameter (or thickness) of a platinum particle. In the present experiments the correction used a d value of 2.0 nm.

Cytochrome aa_3 orientation and concentration in COV

Total COV-incorporated cytochrome oxidase and the orientation of the enzyme were determined by spectrophotometric measurement of the amount of reduction caused by ascorbate and by *NNN'N'*-tetramethyl-*p*-phenylenediamine, in the presence of cyanide and cytochrome *c*, as described by Nicholls et al. (1980).

Table 1 Distribution and orientation of cytochrome *c* oxidase in DEAE-Sephacel fractions

n.d, not determined

Composition: lipid, enzyme and initial ratio (mg/mg)*	DEAE-Sephacel fraction number	Concn. of phosphate buffer at which fraction eluted (mM)	Respiratory control ratio (mean value)	Final lipid/protein ratio (mg/mg)	Turnover (electrons/ aa_3 per s)	Percentage of cytochrome aa_3 facing out
EggPC/PE	FI	25	4.3	945.0	n.d.	13.5
(1:1, w/w) plus	FII	75	13.5	21.0	234	69.0
normal enzyme	FIII	150	8.0	18.6	228	65.5
(L/P = 25)						
Egg PC/PE (1:1, w/w)	FI	25	1.5	209.0	n.d.	15.5
plus normal enzymes	FII	75	2.0	10.0	65	60.5
(L/P = 10)	FIII	150	1.5	4.8	83	82.0
DOPC/DOPE	FI	25	3.2	890.0	n.d.	0.0
(1:1, w/w) plus	FII	75	9.7	27.0	516	54.0
normal enzyme	FIII	150	11.7	18.9	450	63.0
(L/P = 25)						
DOPC/DOPE (1:1, w/w)	FI	25	2.2	1281.0	n.d.	9.0
plus normal enzyme	FIII	150	3.0	5.0	425	70.0
(L/P = 10)						
DOPC/DOPE	FI	25	3.3	n.d.	n.d.	14.0
(1:1, w/w) plus	FIII	150	1.5	n.d.	227	77.0
SUIIID enzyme						
(L/P = 10)						

* L/P ratios in original mixtures before fractionation.

Polarographic measurements of oxygen uptake

Oxygen uptake was measured in air-saturated 50 mM potassium phosphate buffer, pH 7.4, at 30 °C using a Clark-type oxygen electrode (Yellow Springs Instrument Co.) attached to a suitable polarizing box and recorder. Respiratory control ratios were obtained by measuring rates before and after the addition of carbonyl cyanide *p*-trifluoromethoxyphenylhydrazone and valinomycin to the suspension of vesicles in the chamber (Nicholls et al., 1980, 1990).

Phospholipid determination

The amount of phospholipid in the initial suspensions and in the eluted fractions was measured as inorganic phosphate. Phospholipids were extracted by the method of Folch et al. (1957) and then converted into inorganic phosphate by ashing (Ames, 1966) and quantified using an ascorbic acid/molybdate reagent (Chen et al., 1956).

RESULTS

Characterization of vesicles

The elution profiles for reconstituted vesicles fractionated by DEAE-Sephacel chromatography showed three major peaks. The first fraction, FI, comprised protein-free vesicles together with COV containing a very small amount of mainly inward-facing enzyme; these were eluted with 25 mM potassium phosphate buffer, pH 7.4, in all experiments. A second fraction, FII, contained enzyme present in both orientations. These COV were eluted with 75 mM potassium phosphate buffer. In the experiments using DOPC/DOPE (L/P = 10 mg/mg) no FII fraction was obtained. A third protein-containing fraction, FIII, was eluted with 150 mM potassium phosphate buffer.

The distributions and orientations of cytochrome *c* oxidase in these fractions are summarized in Table 1. The L/P ratios for all the FI fractions indicate that only a small amount of enzyme has been incorporated, of which more than 80% is inward-facing. The FII fraction from eggPC/PE mixtures with L/P = 25 mg/mg has the highest respiratory control ratio and contains the 'classic' 70% outward-facing enzyme. L/P ratios for the FIII fractions indicate a greater enzyme incorporation than that expected from the initial L/P ratio for both L/P = 10 mg/mg and L/P = 25 mg/mg COV. This excess of oxidase protein over phospholipid is achieved at the expense of the higher amounts of phospholipid in the FI fractions. There are no differences in enzyme incorporation level between the egg and the dioleoyl phospholipid types.

Similar proportions (65%) of enzyme molecules face outwards in the FIII fractions of both egg and the dioleoyl mixtures at L/P = 25 mg/mg, whereas slightly more is outward-facing in the FIII L/P = 10 mg/mg populations. Each oxidase molecule in the L/P = 10 mg/mg COV will be affected by a greater relative amount of neighbouring protein particles; this may force more of the molecules to adopt an outward orientation. Reasonable respiratory control ratios were measured for all the fractions from the L/P = 25 mg/mg COV, but fractions from the L/P = 10 mg/mg mixtures showed much lower respiratory control ratios. Enzyme turnover (expressed as electron equivalents/mol of cytochrome aa_3 per s) in the fully uncontrolled state was slightly higher in all the DOPC/DOPE COV fractions than in the eggPC/PE L/P = 25 mg/mg COV fractions. Turnover of the enzyme in the eggPC/PE L/P = 10 mg/mg COV (both FII and FIII fractions) was distinctly lower (80 s^{-1}); we do not yet have an explanation for this decreased enzyme activity, which was seen in three different proteoliposomal preparations.

Electron microscopy

Figures 1–4 present electron microscope images of Pt/C replicas of freeze-fractured samples from the several types of COV. In general, our size distributions agree with those of Wrigglesworth (1985).

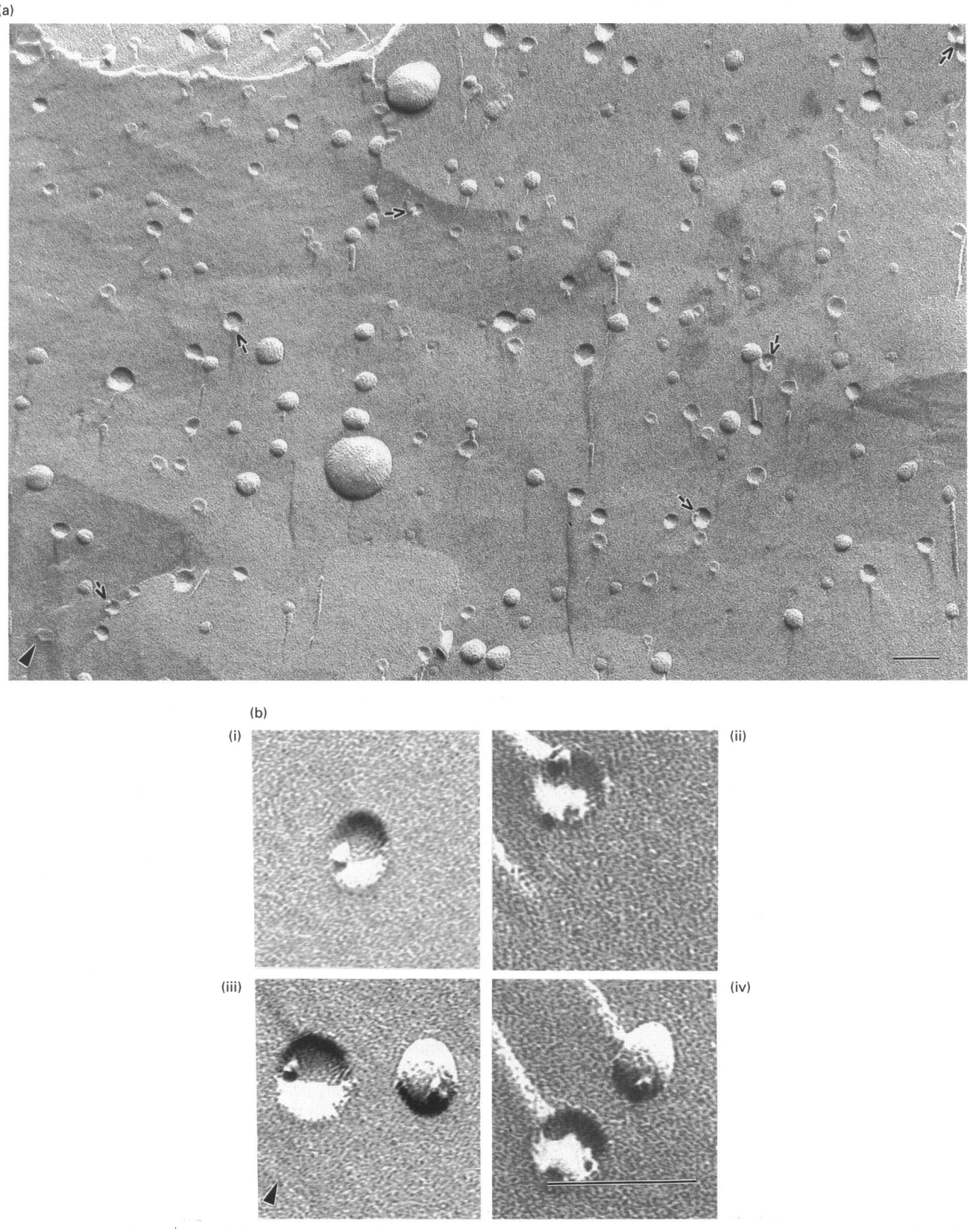

Figure 1 For legend see facing page.

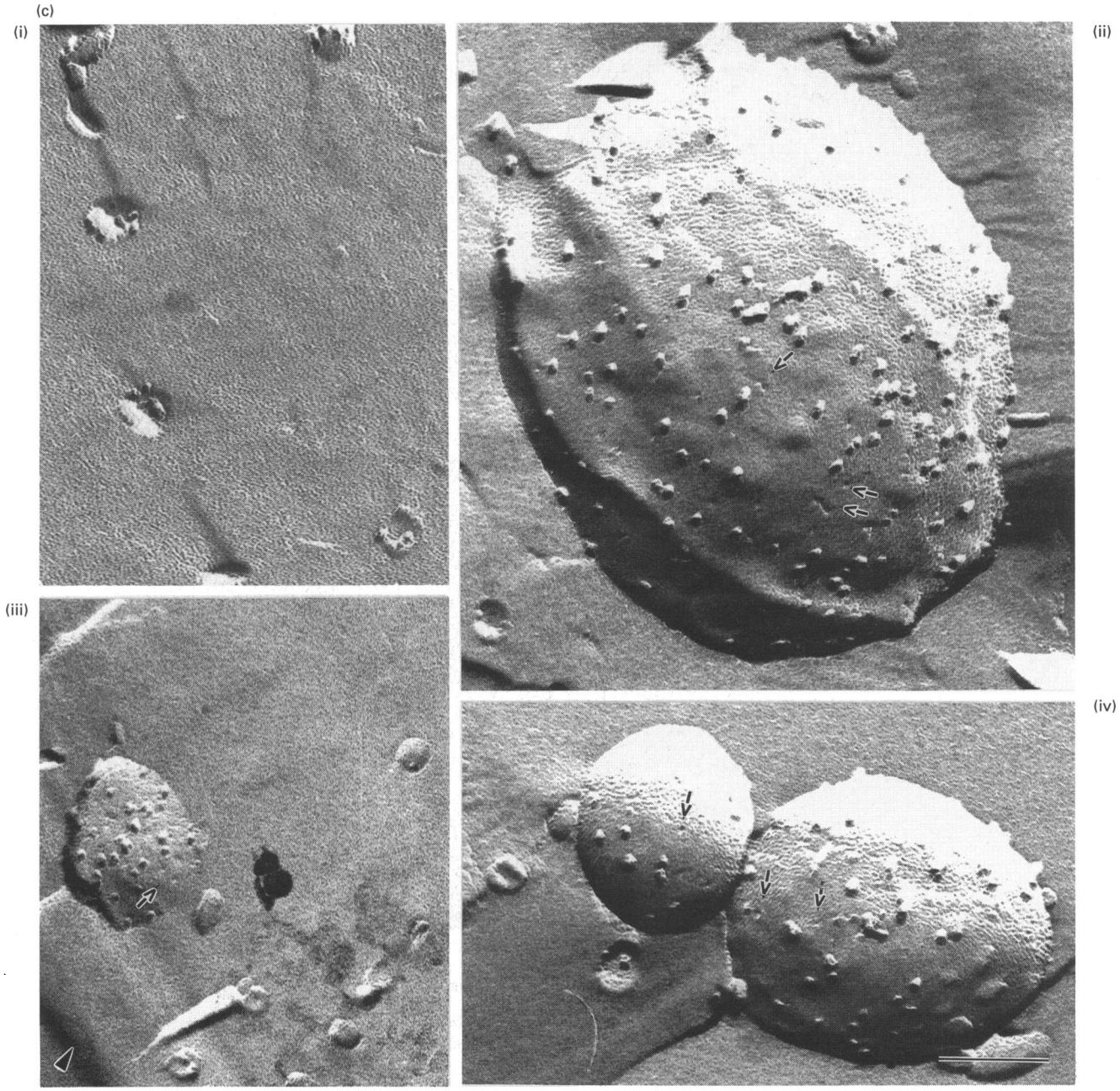

Figure 1 Electron microscopy of eggPC/PE proteoliposomes (initial L/P ratio = 25 mg/mg)

(**a**) Protein-free vesicle fraction (FI). A sample of the minority of vesicles eluted with 25 mM phosphate buffer without binding to the DEAE-Sephacel column is shown. This is the FI fraction containing approx. 95% empty vesicles. A few vesicles contain intramembranous particles (arrows). Bar = 100 nm. (**b**) First protein-containing fraction (FII). Four samples of the vesicles eluted with 75 mM phosphate from the DEAE-Sephacel column are shown. This fraction is more homogeneous than the FIII fraction (cf. **c**). Bar = 100 nm. (**c**) Second protein-loaded fraction (FIII). Four samples of the vesicles eluted with 150 mM phosphate from the DEAE-Sephacel column are shown. The majority (i) have diameters of 20–50 nm. A few larger proteoliposomes occur with diameters of 200–300 nm (iii and iv). Rare examples (ii) are 500 nm or larger. The surfaces show mainly projecting protein with a few shallow hollows (arrows). Irregular shapes may represent different tilts of the particles relative to the membrane surface. The larger particles in particular exhibit irregular shapes. Bar = 100 nm.

Figure 1 illustrates the appearance of the three eluted COV populations obtained from eggPC/PE L/P = 25 mg/mg mixtures. The field in Figure 1(a) shows the essentially protein-free vesicles from the FI fraction. Of these, 95% are empty vesicles with diameters of 20 nm and upwards. A few intramembranous particles can be seen in a minority of slightly larger vesicles (indicated by the arrows). Four examples of vesicles from the FII fraction are presented in Figure 1(b). The fractured surfaces have diameters of 20–50 nm and typically contain one to three enzyme particles. A few larger proteoliposomes with diameters between 50 and 300 nm were also found. Four different freeze–fracture replicas of COV from the FIII fractions are shown in Figure 1(c). The fractured surfaces have apparent diameters up to 50 nm, and are inlaid with one to five enzyme particles (Figure 1c, i). A few large proteoliposomes with diameters up to or even greater than 500 nm were also present (Figure 1c, ii and iv).

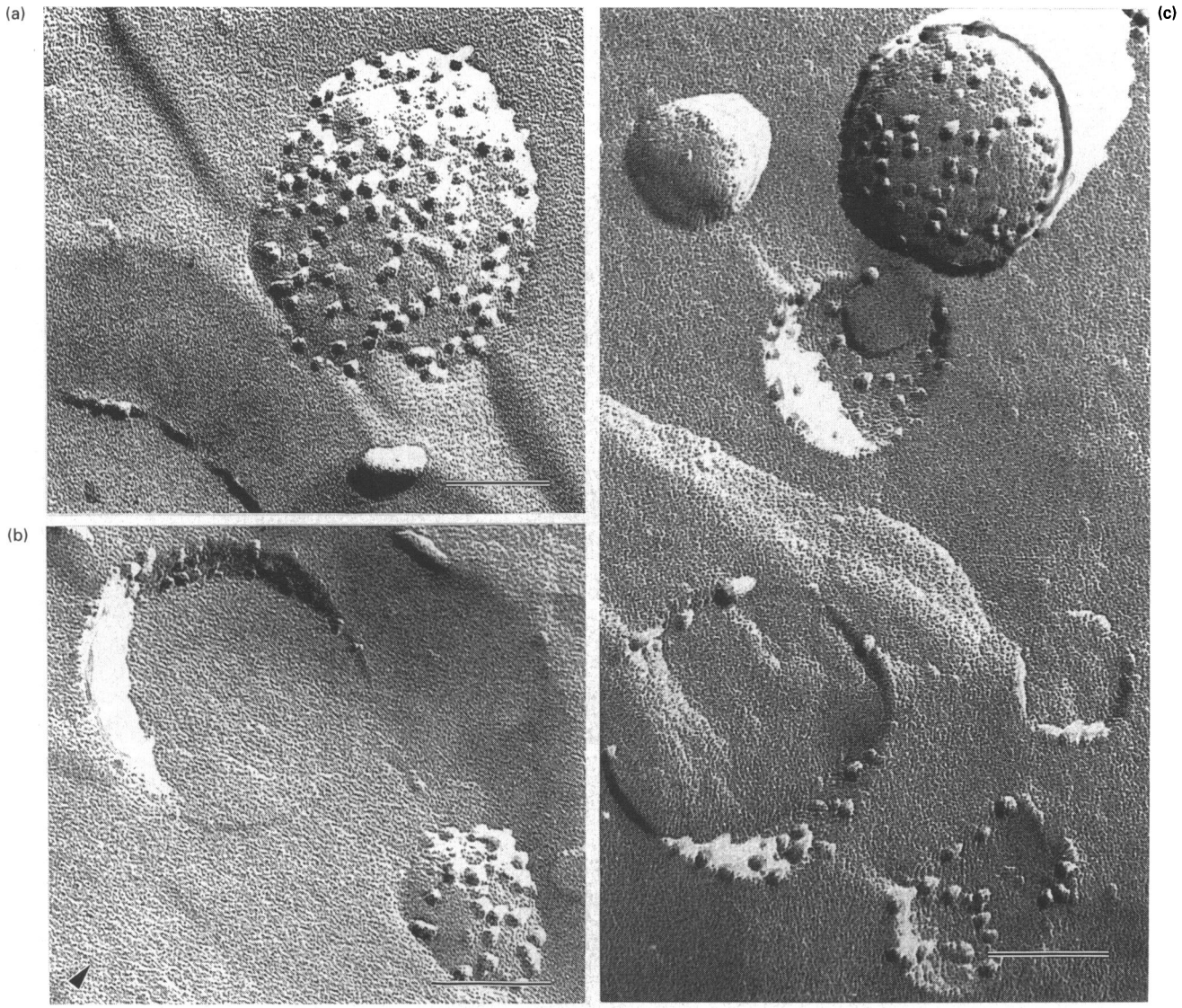

Figure 2 Electron microscopy of eggPC/PE proteoliposomes (FIII, initial L/P ratio = 10 mg/mg)

Three samples of the vesicles eluted with 150 mM phosphate from the DEAE-Sephacel column are shown. This fraction contains larger structures with diameters of 100 nm (**b**) to 250 nm (**a** and **c**). Note the even distribution of enzyme complexes. For comparison with the L/P = 25 mg/mg samples in Figure 1(c). Bar = 100 nm.

The surfaces of all the replicas contain protein-derived projections and a few shallow hollows where particles were removed during fracturing (see the arrows in Figure 1c, iii and iv). Most of the expected hollows. including all the smaller ones, are probably covered with shadowing metal which prevents their detection. The projections are predominantly rounded. Some other shapes may represent tilting of the original molecules relative to the membrane plane. Larger (oligomeric?) particles (see Figure 1c, ii and iv) are irregular. A few multilamellar aggregates (both with and without incorporated protein particles) were also found in these egg phospholipid-derived proteoliposomes.

Figure 2 shows the appearance of the FIII COV fraction obtained from the eggPC/eggPE L/P = 10 mg/mg mixture. Such vesicles are markedly larger than COV at higher L/P ratios, and have apparent diameters of between 100 and 250 nm (Figures 2a and 2c). A relatively even distribution of the presumed enzyme complexes can be seen in the example presented in Figure 2(a). Such COV of the FIII fraction type are in general more heterogeneous than those in the FII fractions. Figure 2 contains examples of both convex and concave fracture faces (Figure 2c) as well as some possible cross-fractures.

Figures 3 and 4 contain images of replicas from proteoliposomes prepared using DOPE/DOPC phospholipid mixtures. In Figure 3 we see FIII proteoliposomes from the FIII fraction of the DOPE/DOPC L/P = 25 mg/mg mixture. These have a similar morphology to that of COV in the corresponding fraction from the egg phospholipid mixture. Most of these dioleoyl phospholipid COV are relatively small (Figure 3a) but a few are seen that are larger than 500 nm in diameter (Figure 3b). Incorporation at an L/P = 10 mg/mg ratio using DOPE/DOPC gave the populations of COV shown in Figure 4. Their morphology resembles that seen in the corresponding DOPE/DOPC L/P = 25 mg/mg COV, rather than the more 'crowded' pattern of the eggPE/PC L/P = 10 mg/mg COV (Figure 2). Most vesicles have diameters between 20 and 50 nm with a few larger

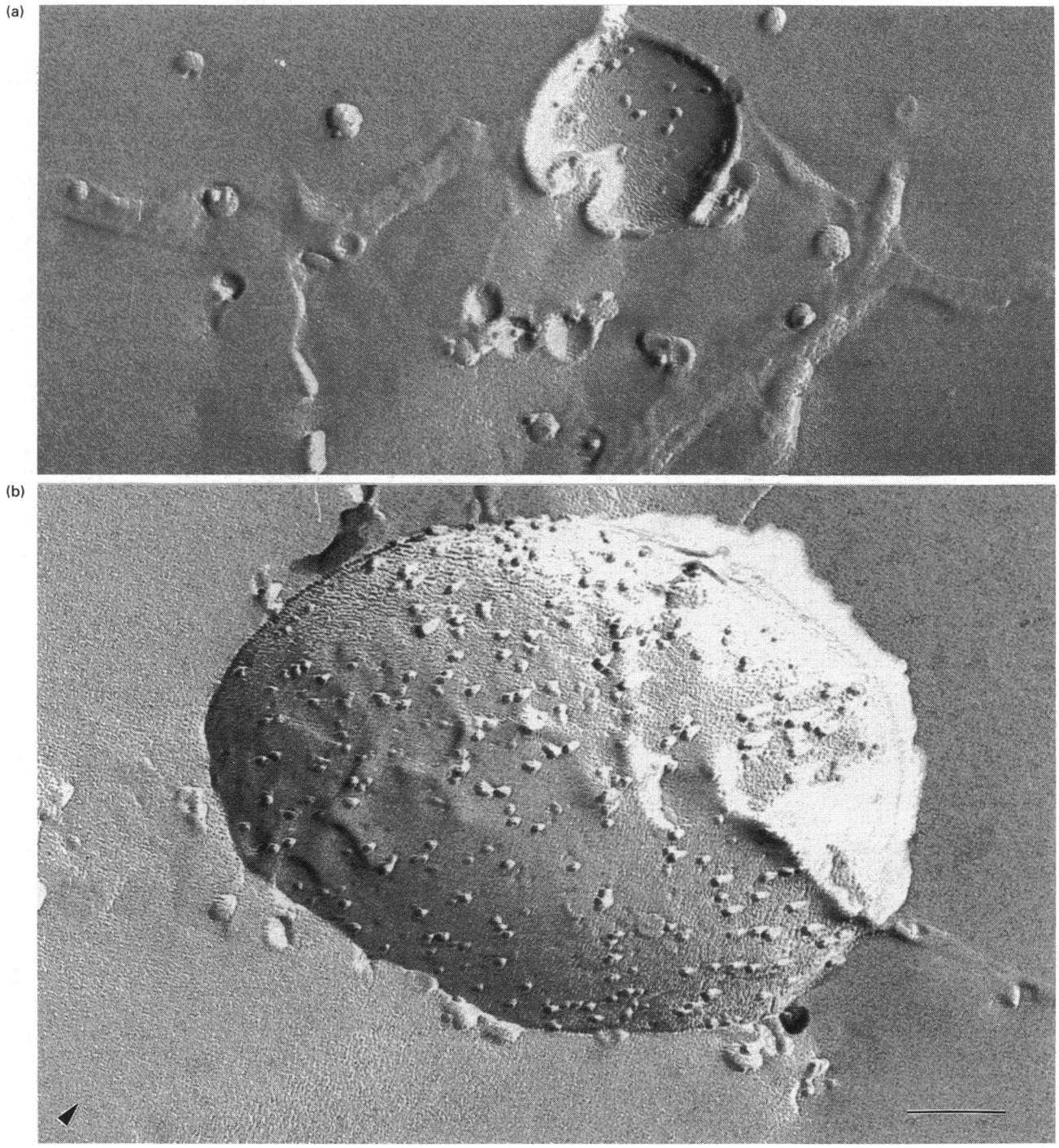

Figure 3 Electron microscopy of DOPC/DOPE proteoliposomes (FIII, initial L/P ratio = 25 mg/mg)

Two samples of the vesicles eluted with 150 mM phosphate from the DEAE-Sephacel column are shown. (**a**) The smaller forms; (**b**) a larger form. These proteoliposomes have a similar morphology to that of the eggPC/PE fraction in Figure 1(c). Bar = 100 nm.

exceptions as illustrated in Figure 4(a). Unlike the eggPC/PE-derived COV, the L/P ratio of the DOPE/DOPC-derived vesicles has little influence upon vesicle size.

These results thus show that COV are still somewhat heterogeneous, even when prepared from defined lipids by dialysis and fractionated (cf. Wrigglesworth et al., 1987). The proportion of large COV detected by electron microscopy may be even less than that in the original suspensions because not all of the vesicles are fractured equatorially. In every proteoliposome fraction from both egg and dioleoyl phospholipid mixtures some smooth and particle-free fracture surfaces were observed. This suggests not only that vesicle size is variable but also that protein incorporation is not entirely random.

Calculations and measurements of the proportions of protein-

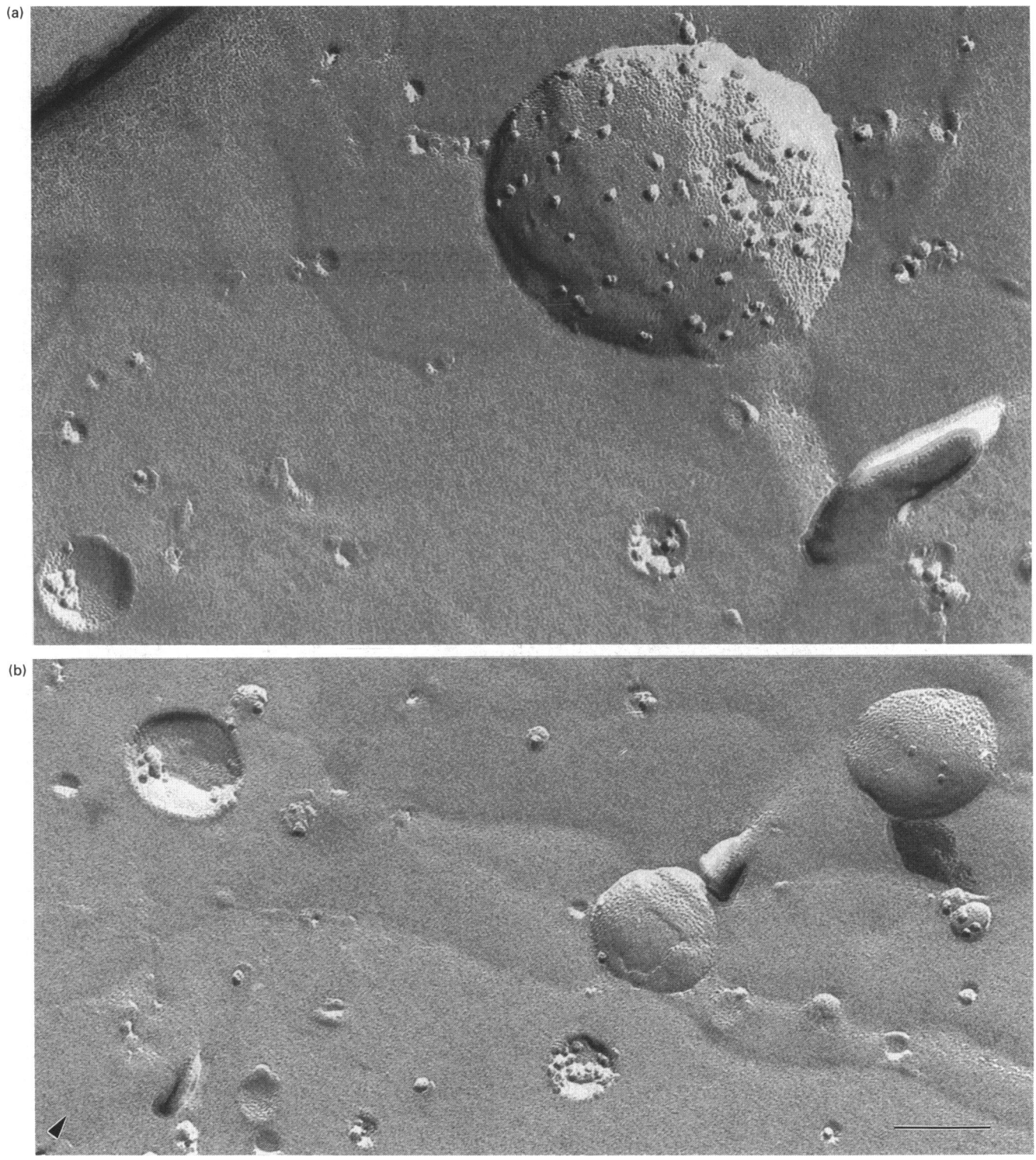

Figure 4 Electron microscopy of DOPC/DOPE proteoliposomes (FIII, initial L/P ratio = 10 mg/mg)

Two samples of the vesicles eluted with 150 mM phosphate from the DEAE-Sephacel column are shown. Compare with the L/P = 25 mg/mg group (Figure 3), and contrast with the corresponding L/P = 10 mg/mg eggPC/PE mixture (Figure 2). The majority of vesicles have diameters of 20–50 nm (**b**) with a few larger structures (**a**) as illustrated. Bar = 100 nm.

covered vesicle area were carried out for all the FIII fractions. The values obtained by measurement using the image analyser system and by theoretical calculation are listed in Table 2. The method for deriving the 'theoretical' protein-covered area is outlined in the Discussion section. No significant differences in the measured particle-covered areas between small and large vesicles were seen. The COV from DOPC/DOPE L/P = 25 mg/mg mixtures have a slightly greater proportion of particle-covered area than do the COV from eggPC/PE mixtures. If the starting L/P ratio is 10, the percentage of outward-facing particles

Table 2 Measurement and calculation of protein-covered areas in COV

Fraction III: lipid type, protein type and initial L/P ratios (mg/mg)*	Observed protein-covered areas: convex faces†	Observed protein-covered areas: concave faces†	Calculated protein-covered area (C-side of oxidase)‡
eggPC/PE L/P = 25	0.087	Not determined	0.026
eggPC/PE L/P = 10 (control enzyme)	0.141	0.177	0.101
DOPC/DOPE L/P = 25	0.093	Not determined	0.026
DOPC/DOPE L/P = 10 (control enzyme)	0.117	0.150	0.094
DOPC/DOPE L/P = 10 (SUIIID enzyme)	0.146	0.146	Not determined

* L/P ratios in original mixtures before fractionation (see Table 1 for final ratios).
† From a count of protein projections multiplied by the average area.
‡ From the L/P ratio (Table 1) assuming a bilayer structure for the COV, with average surface areas of 0.6 nm^2 per phospholipid and 37 nm^2 per oxidase monomer (see the Discussion and Table 4).

is higher for eggPC/PE COV than for DOPC/DOPE COV (Table 1). Similarly, the proportion of particle-covered area (Table 2) for eggPC/PE COV is higher than for DOPC/DOPE COV. In COV from both phospholipid mixtures the relative protein-covered areas are lower on convex fracture surfaces than on the corresponding concave fracture surfaces.

SUIII-depleted enzyme

The enzyme was depleted of subunit III (as well as some smaller subunits) as described in the Materials and methods section. The Soret maximum in the u.v.-visible absorption spectrum of the oxidized 'resting' enzyme at 418 nm shifts to approx. 422 nm after this subunit depletion. Such a shift resembles that which occurs upon 'pulsing' reduced enzyme with oxygen, although the pulsed enzyme does not seem to lose any of its subunits (Crinson and Nicholls, 1992). SUIII-depleted cytochrome aa_3 subsequently incorporated into DOPC/DOPE-derived proteoliposomes at an L/P ratio of 10 mg/mg gave rise to two fractions after DEAE-Sephacel separation (see Table 1). COV in the FIII fraction with

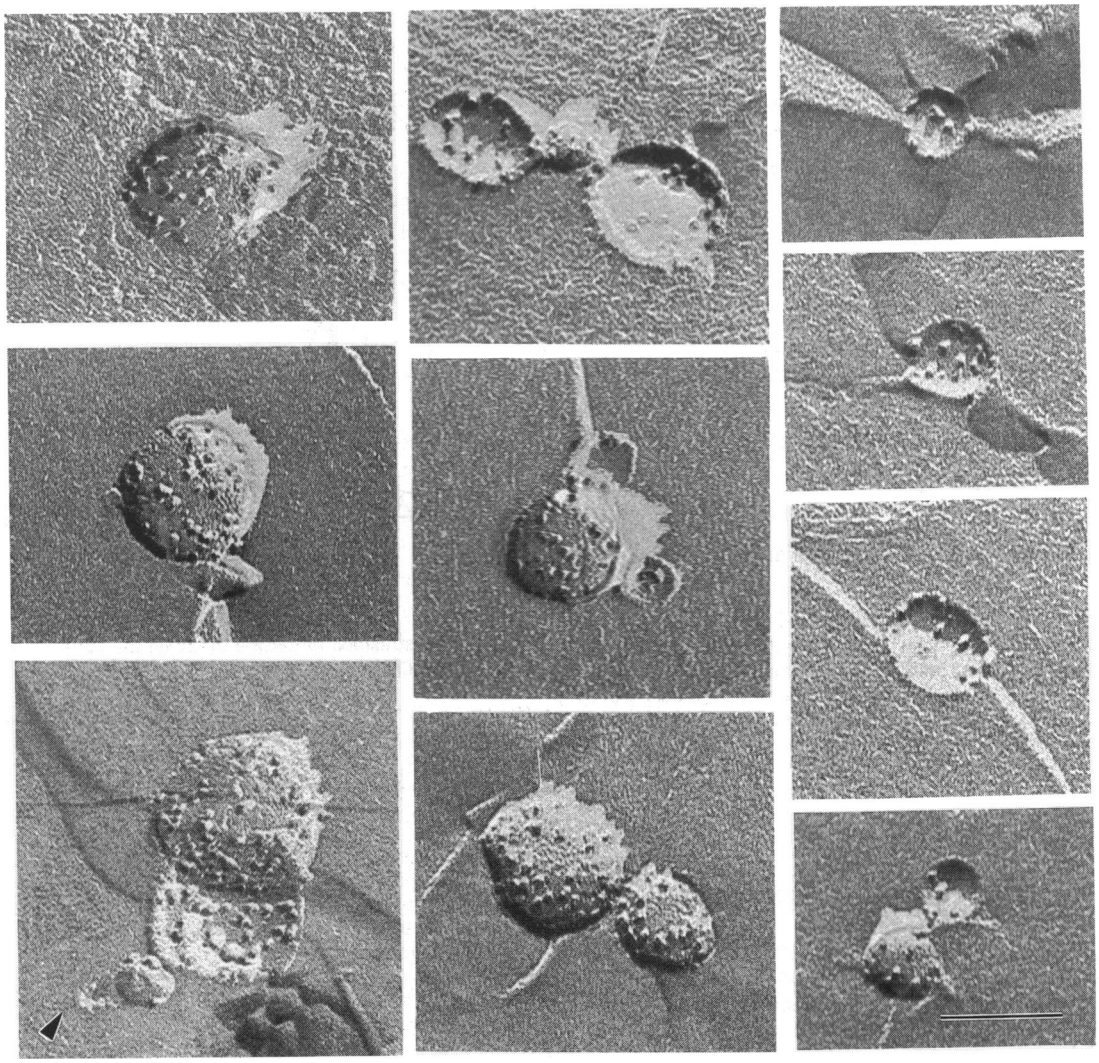

Figure 5 Electron microscopy of DOPC/DOPE proteoliposomes (initial L/P ratio = 10 mg/mg, SUIII-depleted protein)

Ten samples of FIII vesicles eluted with 150 mM phosphate from the DEAE-Sephacel column are shown. SUIII-depleted aa_3 was incorporated into DOPC/DOPE (1:1, w:w) liposomes at L/P = 10 mg/mg. Average diameter of the vesicles is 30–60 nm. SUIII-depleted enzyme projections on both convex (left and centre panels) and concave (right panels) fracture faces are more heterogeneous than with undepleted enzyme (cf. Figure 4). Bar = 100 nm.

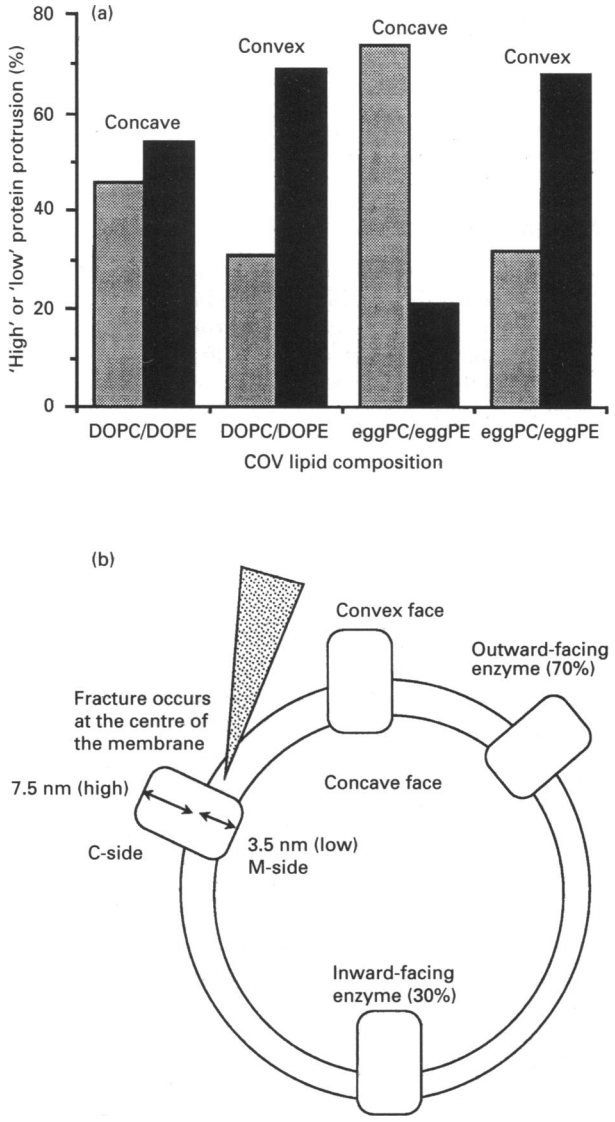

Figure 6 Average heights of oxidase projections on convex and concave fracture faces

(**a**) Summary of the data from DOPC/DOPE ($n = 73$) and eggPC/PE COV ($n = 107$), with an initial L/P ratio = 10 mg/mg. N.B. two types of protein protrusion: 'high' (7.5–8.0 nm, the presumed C-face; ■) and 'low' (3.0–3.5 nm, the presumed M-face; ▨). High/low ratio for convex surfaces is approx. 70:30. (**b**) A schematic representation of the asymmetrical transmembrane location of cytochrome *c* oxidase. As fracturing occurs at the bilayer centre, 2.0 nm should be subtracted from each high and each low value for a bilayer 4.0 nm thick. The average corrected heights are 5.5–6.0 nm (C-faces) and 1.0–1.5 nm (M-faces).

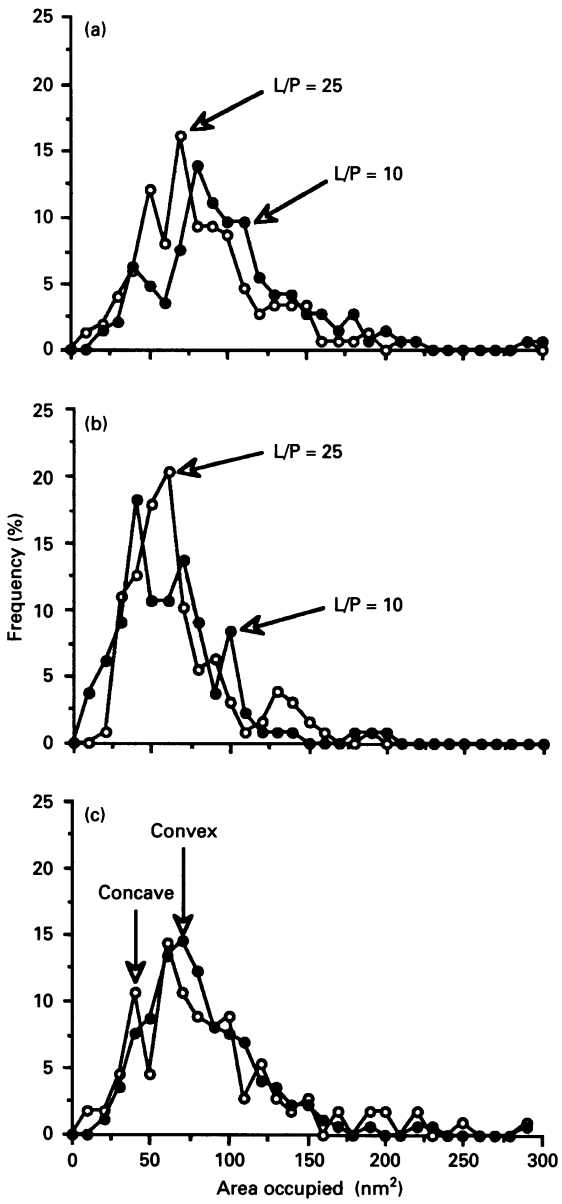

Figure 7 Distribution of particle areas on the surfaces of eggPC/PE and DOPC/DOPE COV

(**a**) EggPC/PE COV [initial L/P ratios = 10 mg/mg (●; $n = 144$) and 25 mg/mg (○; $n = 149$)]. The smallest particles of area 30–50 nm^2 form the first peak and the most abundant particles have an average area of 70 nm^2 in both cases. Larger particles may represent aggregates. Data are for convex fracture faces. (**b**) DOPC/DOPE COV [initial L/P ratios = 10 mg/mg (●; $n = 132$) and 25 mg/mg (○; $n = 128$)]. The most abundant particles have areas 60–70 nm^2 with a smaller number at 30–40 nm^2. Larger particles may represent aggregates. No very large (approx. 300 nm^2) aggregates were found. Data are for convex fracture faces. (**c**) Comparison of concave and convex fracture faces, DOPC/DOPE COV (initial L/P ratio = 10 mg/mg). The 40 nm^2 area particles may be more numerous on concave than on convex faces of the bilayers. The most numerous population on the concave faces (○; $n = 109$) has an average area approx. 60 nm^2 (possibly representing M-sides of dimers). On the convex faces (●; $n = 139$) in this preparation the most numerous population has an average area closer to 70 nm^2 (possibly representing C-sides of dimers). Data are from one COV preparation (cf. summary in Table 4).

SUIII-depleted enzyme contained more outward-oriented particles than did those in a control FIII fraction prepared using an undepleted sample of enzyme.

Freeze–fracture replicas of proteoliposomes from such an FIII fraction containing SUIII-depleted enzyme are illustrated in Figure 5. These COV are typically between 30 and 60 nm in diameter, but some COV up to 250 nm in diameter (as well as a few larger than 500 nm) were also found (not shown). Examples of protein-derived projections on both convex fracture surfaces (left hand panels in Figure 5) and concave fracture surfaces (right hand panels in Figure 5) are shown. These protein projections, on both surfaces, are more heterogeneous in shape than those obtained with control (undepleted) enzyme COV (see Figure 4).

The proportion of protein-covered area in COV prepared with SUIII-depleted enzyme was similar for the convex and concave faces (these data are summarized in Table 2).

Table 3 Average surface areas (nm^2) of enzyme particles: convex faces, FII and FIII fractions

The calculated areas are individual areas according to the model in the text (cf. Tables 2 and 4).

DOPC/DOPE, L/P = 25*		DOPC/DOPE, L/P = 10*		EggPC/PE, L/P = 25*		EggPC/PE, L/P = 10*			Calculated area (nm^2)	
Size (nm^2)	%	Size (nm^2)	%	Size (nm^2)	%	Size (nm^2)	%		C-side	M-side
40±10	41†	40±10	38†	40±10	22	40±10	13	Monomer	37	21.5
70±10	36	70±10	33	70±10	34†	70±10	25	Dimer	74	43
100±10	10	100±10	14	100±10	23	100±10	31†	Tetramer	148	86
140±20	11	140±20	2.3	140±20	13	140±20	20	Hexamer	222	129

* L/P ratios in original mixtures before fractionation.
† Most common particles size.

Table 4 Dimensions of membrane-bound cytochrome oxidase

Parameter	Reconstituted COV*		Quasi-crystal form	
	Type A (concave)	Type B (convex)	1979–82†	1990‡
Larger areas (nm^2)	60.0	70.0	50–60	28.0
Smaller areas (nm^2)	30.0	40.0	–	–
SUIII-depleted (nm^2)	10.0–30.0		–	–
Total length (nm)	11.0		12.0	
C-domain height (nm)	5.5		6.0	
M-domain height (nm)	1.5–2.0		2.5	

* Data from this paper.
† Data from Frey et al (1982) and Fuller et al. (1979).
‡ Data from Valpuesta et al. (1990).

Particle heights and size distributions

The height distributions of the protruding particles exhibit substantial variation. Figure 6 summarizes the heights measured in convex and concave faces from replicas of COV prepared with both egg and dioleoyl phospholipid mixtures (at an L/P ratio = 10 mg/mg). Two size families of protrusion are seen, the first about 7.5 nm and the second about 3.5 nm high. The approx. 7.5 nm knobs may represent the 'C'-faces and the approx. 3.5 nm knobs the 'M'-faces of the original embedded molecules. In COV from eggPC/PE mixtures more 'high' knobs seem to occur on the convex faces, and more 'low' knobs on the concave faces. In COV from DOPC/DOPE mixtures a rather greater proportion of 'high' knobs was seen on the convex faces, but the distribution on the concave faces appeared to be approximately even.

Since fracturing occurs at the centre of the membrane, 2.0 nm should be subtracted from each value for a membrane of 4.0 nm thickness in order to obtain the height of the original projecting species if it were measured from the phospholipid head group region (as illustrated in Figure 6b). An average *in situ* projecting height of 5.5–6.0 nm is obtained in this way for the presumed cytosolic 'half' of the complex and a corresponding height of up to 1.5 nm for the presumed matrix 'half' of the complex. These values resemble those originally calculated for the C domain (approx. 6.0 nm) and for the M arms (approx. 2.5 nm) in the case of the partially crystalline form studied by Frey et al. (1982).

The image analysis system described in the Materials and methods section was used to determine particle areas and size distribution profiles for the reconstituted enzyme preparations. The results produced are summarized in Figure 7. Equal numbers of particles were measured in each experiment. The size of each projection has been corrected for the contribution of the platinum particles involved, according to the procedure given in the Materials and methods section [eqn. (1)]. The resulting size distribution profiles do not have well-defined peaks but show patterns which may correspond to populations with certain discrete values.

In COV from eggPC/PE mixtures (Figure 7a), the smallest particles have areas of between 30 and 50 nm^2, and the most numerous particles have areas of between 70 and 80 nm^2. Particles with areas $\geqslant$ 100 nm^2 may represent aggregates. The COV from L/P = 10 mg/mg and L/P = 25 mg/mg ratio mixtures have similar profiles with a slightly greater proportion of larger particles being seen at the L/P = 10 ratio. In the case of COV from DOPC/DOPE mixtures (Figure 7b), the most common proteoliposome type has a rather smaller average area than in COV prepared with egg phospholipids. The most numerous COV among those prepared from DOPC/DOPE mixtures at L/P = 25 mg/mg have an average area of 60–70 nm^2. A smaller population occurs with areas of 30–40 nm^2. The size distributions of the DOPC/DOPE COV differ from those of the eggPC/PE COV. Larger structures again presumably represent aggregates. The very smallest structures (with areas approx. 30 nm^2) are more numerous in DOPC/DOPE-derived vesicle populations than in eggPC/PE vesicle populations.

Figure 7(c) compares the areas of projections in a single vesicle preparation prepared with DOPC/DOPE at a L/P = 10 mg/mg, measured on the two COV fracture faces. Smaller particles may be slightly more numerous on the concave than on the convex halves. The most numerous group on the concave faces has an average area of between 40 and 60 nm^2. This may represent the M-faces of dimeric complexes (see the Discussion section). On the convex faces the most numerous population has an average area closer to 70 nm^2. Such a population may represent the C-faces of dimeric complexes. However, in general, the relative distributions on the two faces are not significantly different.

Table 3 summarizes our interpretation of the results presented in Figure 7. It assumes that there exist well-defined populations of particles in terms of size. The particles in the two COV fractions from eggPC/PE mixtures exhibit larger average areas than those in the corresponding DOPC/DOPE proteoliposome fractions. For each phospholipid mixture there may be some larger particles in the COV from L/P = 10 mg/mg mixtures than in the COV from L/P = 25 mg/mg mixtures. The enzyme

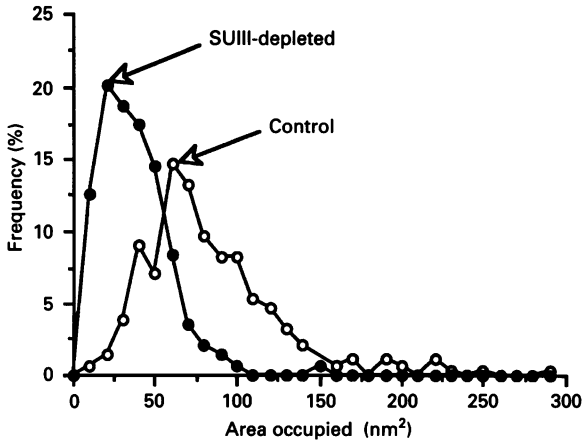

Figure 8 Size distributions of protein projections on DOPC/DOPE COV for SUIII-depleted and control enzyme (initial L/P ratio = 10 mg/mg)

SUIII-depleted enzyme occupies approx. 50% of the surface area of undepleted enzyme. Frequencies are calculated for both fractured surfaces. SUIII-depleted enzyme particles (●; $n = 144$) show a frequency profile with a maximum at 20 nm² and a shoulder at 40 nm². Undepleted enzyme particles (○; $n = 139$) show a frequency profile with a peak or peaks in the 40–60 nm² region.

complexes may change their aggregation state and possibly their conformations during the process of incorporation (see the Discussion section and Table 4).

An analysis of the areas of projections in replicas of COV prepared with SUIII-depleted enzyme (using DOPC/DOPE mixtures at an L/P ratio of 10 mg/mg) was also carried out. Figure 8 shows the resulting distribution of projecting complexes as a function of area for such SUIII-depleted samples, compared with the distribution for the corresponding COV prepared with control (undepleted) enzyme. Areas were calculated for both fracture faces. The SUIII-depleted enzyme particles show a profile with a maximum between 20 and 40 nm². On average, these particles have approximately half the surface area of those with undepleted enzyme, which show a peak at 60 nm². Very few larger units, representing aggregates, were observed in COV with SUIII-depleted enzyme. The size distribution profile is thus substantially different from that of the control. The protein-covered area in such COV is listed in Table 2. It is also higher for COV with SUIII-depleted enzyme than for COV with undepleted protein particles under similar experimental conditions. Our COV with SUIII-depleted enzyme, however, did not show substantial respiratory control ratios (see Table 1).

DISCUSSION

The following structural parameters have been investigated: (i) the areas of individual enzyme particles viewed from the convex and concave side of the proteoliposomal membrane; (ii) the heights of the individual enzyme particles at the two faces; (iii) the size distributions of the individual enzyme particles; and (iv) the proportion of protein occupancy in the membranes, i.e. the total protein-covered area. We sought to identify differences that may be induced by (a) variations in phospholipid composition, as represented by the dioleoyl moiety (DOPC/DOPE) compared with the more saturated hydrophobic fatty acid side chains in egg phospholipid bilayers, (b) different initial ratios of phospholipid to protein and (c) different states of the protein, as represented by the SUIII-depleted system.

The characteristic DEAE-Sephacel elution of at least three fractions indicates that enzyme is unevenly incorporated into the liposomes forming during detergent removal from the dialysing mixture. No significant correlations were found between liposome size and the level of protein incorporation. Several varieties of COV were found within each of the DEAE-Sephacel fractions, including: (i) smaller and larger empty vesicles; (ii) smaller and larger vesicles with few particles; (iii) smaller and larger proteoliposomes with numerous particles; and (iv) some multilayered aggregates (in the DOPC/DOPE COV) with and without incorporated protein. The vesicles containing numerous particles form the largest proportion of COV in the FIII fractions. In such COV the oxidase complexes are relatively evenly distributed, as found by Wrigglesworth (1985).

With egg phospholipid mixtures, larger vesicles were obtained as the phospholipid to protein ratio decreased. This agrees with the size distributions calculated from similar micrographs by Madden et al. (1983). With DOPC/DOPE mixtures, the phospholipid to protein ratio had little influence on vesicle size. Although enzyme was incorporated at a higher surface concentration, the presence of more protein particles did not cause liposome enlargement. Possibly the average dimensions of the inlaid protein complexes rather than their total amount may be the critical factor determining vesicle size. Proteoliposomes (FIII) from egg phospholipids at an L/P ratio of 10 mg/mg had the largest number of aggregates and the greatest protein-covered area (cf. data in Tables 2 and 3). If protein incorporates into the bilayer before the membrane sheets fragment into smaller vesicles (Wrigglesworth, 1988; Wrigglesworth et al., 1987), then the particle size and location as well as (sometimes) the total amount of protein will determine vesicle size.

The enzyme molecules may preferentially incorporate as dimers, as indicated by the percentages seen for the smaller populations in Table 3. A non-bilayer-forming unsaturated lipid such as DOPE can act as a focus for fusion with a membrane protein (Wrigglesworth, 1988). More large complexes were found in COV formed with egg phospholipids, the saturated fatty acyl side chains of which may favour aggregation of the protein beyond the dimeric state. But none of the observed structural differences appear to affect the functional characteristics and activity of the enzyme (see Table 1).

The total membrane area occupied by the enzyme incorporated at the highest levels used here would not seem to be large enough to constrain its orientation within the bilayers. However, COV with higher levels showed diminished respiratory control ratios (see Table 1). Madden et al. (1984) found that optimum respiratory control occurred when there was only one oxidase complex (dimer?) per vesicle, and suggested that in vesicles with two or more dimers the inward-oriented oxidase could decontrol outward-oriented oxidase. Cooper and Nicholls (1990), however, showed that cytochrome *c*-loaded COV are structurally indistinguishable from standard COV and can generate a significant protonmotive force with an orientation either the same as or opposite to that generated in standard COV with externally facing oxidase. Our results indicate that a high control ratio requires an L/P ratio greater than 10 mg/mg (Table 1). Populations of vesicles with appreciable amounts of inward-oriented oxidase but with substantial L/P ratios can show high respiratory control ratio values. Vesicles with large amounts of outward-facing cytochrome aa_3 but smaller L/P ratios show very low respiratory control ratios. The differences may reflect the different proton permeabilities close to the inlaid enzyme complexes, but a full explanation will require further study of the properties of the COV involved.

At physiological temperatures, the oxidase complexes may

move ('pitch' or 'roll') relative to the membrane plane; such behaviour may be affected by changes in phospholipid composition and the L/P ratio. DOPC/DOPE bilayers are more fluid than eggPC/PE membranes, which favours more rotational freedom and hence more disorder during enzyme incorporation and sample preparation. At lower L/P ratios, enzyme particles are more densely packed which may lead to some restricted mobility. Such conditions may also cause aggregation. Reconstitution with either dioleoylphosphatidylcholine or dioleoylphosphatidylethanolamine alone give COV with somewhat lower enzyme activity. With mixtures, tightly controlled proteoliposomes are obtained (Madden et al., 1983). However, enzyme activities are not significantly affected by different molar ratios of the two phospholipids. The electron flux is a more rugged enzyme parameter than its control by membrane potential and pH gradient.

The expected distributions, areas and particle sizes can be estimated from a knowledge of the protein structure. The oxidase is a molecule with a molecular mass of 200 kDa (Capaldi et al., 1987). A volume of 265–270 nm^3 can be calculated for such a molecule with a specific volume of 0.73. This volume is contained in three domains, one within and two outside the membrane. Approximately 26–28 α-helices span the membrane, with a minimum area requirement of about 0.825 nm^2/helix [see review by Cooper et al. (1991)]; at least 21.5 nm^2 must therefore be set aside for the transmembrane components. Valpuesta et al. (1990) were able to distinguish a cross-sectional area of approx. 14 nm^2 in their images, but the contour level at which this area is measured was rather arbitrary, and the estimate might have increased if the structure had been examined at high resolution. The noise level in the images is probably largely caused by molecular disorder in the crystals. Nevertheless, it is also possible that intrinsic disordering of some helices occurs. A lower than theoretical cross-sectional area would be consistent with two-thirds of the helices being more ordered and one-third more disordered. As not only subunit III, but also subunits VII, VIII and XI, are removed by treatments such as that used here to form SUIII-depleted enzyme, their associated transmembranous helices (up to nine in total) may conceivably be more disordered.

Our particulate projections have predominantly rounded appearance. Cooper et al. (1990) point out that, although cytochrome oxidase is made up of bundles of helices, if a large portion of the polypeptide lies outside the membrane, the extrinsic structure may resemble that of a globular protein. If it is assumed that a 5.5 nm aqueous domain projects from the 'C' side and a similar 1.5 nm domain from the 'M' side of the membrane, an elementary geometrical calculation can be carried out for the volumes and areas of the extra- and intra-membranous parts of the enzyme molecule. A spheroid intersecting the membrane surface with an area, $A = 21.5$ nm^2, on the C side and a cylindrical projection of 1.5 nm in length on the M side will require volumes of 150 nm^3 for the aqueous C-side domain, 86 nm^3 for the transmembrane domain and 32 nm^3 for the aqueous M-side domain (M). The calculated membrane-covered area for a monomeric enzyme molecule at the C-face is then approx. 37 nm^2, based upon the largest cross-section concerned. This value has been used to calculate the theoretical protein-covered areas listed in Table 2, as well as the expected sizes of monomeric, dimeric and higher aggregates in Table 3.

The assignment of molecular orientations and monomer or dimer status to given images nevertheless remains uncertain. Table 3 shows that an observed area of 35–45 nm^2 can be assigned to either the M-face of a putative dimer or the C-face of a putative monomer. The dramatic changes in the pattern of areas with SUIII-depleted enzyme (Figure 8) suggest that nearly all these are due to monomers and therefore essentially all the projections seen with undepleted enzyme samples are due to dimers. The dominant 60–70 nm^2 population in Table 3 would then be identified with the C-faces of dimers, and the particles with mean size 30–40 nm^2 with the M-faces of dimers.

Coexistence of oxidase dimers with larger aggregates as well as with monomers has been observed at low concentrations of Triton X-100 by Robinson and Talbert (1986). Madden and Cullis (1984) claim that standard oxidase isolation techniques produce heterogeneity in subunit composition. The negative staining method of Seki and Oda (1970) showed oxidase particles polymerizing gradually during storage. Polymerization was usually of a linear type. Significant structural heterogeneity and variation between samples of cytochrome oxidase prepared by different methods are reported by Naqui et al. (1984). The larger projections we observe can thus easily be accommodated as tetramers and hexamers, as indicated in Table 3.

One of the roles of subunit III may be to stabilize dimers of cytochrome *c* oxidase (Capaldi et al., 1983; Nalecz et al., 1985; Wilson and Prochaska, 1990). Its removal prevents reassociation of monomers to dimers (Capaldi et al., 1983). The population of particles with an average area of 20 nm^2 in the COV prepared with SUIII-depleted oxidase (Figure 8) is about a third of the total. According to our calculations, these represent the M-faces of depleted and monomerized enzyme on both concave and convex surfaces. The particles with areas $\geqslant 60$ nm^2 comprise a quarter of the total protein. According to the values in the end columns of Table 3, these particles should possibly represent undepleted dimer forms. The remaining particles with areas between 30 and 40 nm^2, which provide nearly half the total area then represent the C-faces of the monomers created by the detergent treatment and subunit removal.

The thickness of the platinum layer is too high to resolve any surface details, and a correction formula was needed to generate the results presented. The values obtained therefore have a relative rather than an absolute meaning. With this caveat in mind, the dimensions obtained for reconstituted cytochrome oxidase molecules are summarized in Table 4, which compares the values for oxidase dimensions measured and calculated here with some obtained previously. Average sizes of the particle shadows on both concave and convex faces confirm the previously reported asymmetry. The high to low ratio of between 65 and 70% for the convex surfaces of both eggPC/PE and DOPC/DOPE vesicles (Figure 6) matches the percentage cytochrome aa_3 facing out obtained spectrophometrically (Table 1). However, the ratios obtained from the concave surfaces are less satisfactory. In some cases the surface used for measurement may have been at an angle different from 45°. The shadows would not then correspond to the heights. It is also possible that the enzyme can adopt different tilts relative to the membrane plane, complicating height measurements more than area determinations.

A number of anomalies remain to be explained. For example, on the concave surfaces the frequency for 30–40 nm^2 particles is low, and on the convex halves of the bilayers these particles are also small in number. Some members of the expected M-face populations are therefore missing. The enzyme aggregates in the vesicles from the initial L/P = 25 mg/mg mixtures give anomalously high values for the total protein-covered area (Table 2). Do the oligomers polymerize in asymmetrical clusters which expose larger than expected areas on their matrix sides? Some of the shapes seen may reflect different patterns of polymerization, possibly linear- or cluster-like (see Seki and Oda, 1970).

In the vesicular 'crystals' of Frey et al. (1982), which were also studied using Pt/C-shadowed freeze–fracture replicas, the C-face of the presumed dimeric complexes contained two structural

domains, probably indicating the location of the monomers. These 'C' domains are largest at the membrane surface and terminate in smaller subdomains (cf. Deatherage et al., 1982a,b). These domains extended 6 nm from the bilayer surface and were separated by between 7 and 8 nm in the presumed dimer. At the M-face the monomers each showed two M domains, M1 and M2, with the M2 arms separated by 3.6 nm and the M1 arms being about 7.0 nm apart. The present results are compared in Table 4 with the dimensions obtained for such semicrystalline forms of the enzyme (Henderson et al., 1977; Fuller et al., 1979; Frey et al., 1982; Valpuesta et al., 1990). The most recent structure for ice-embedded vesicle crystals has a very compact hydrophobic region, in which separate M1 and M2 domains cannot be distinguished. The central membrane area covered by the dimer is small and the total volume detected is only about 50% of that expected for a dimer (Valpuesta et al., 1990). Our freeze–fracture replicas may see more of the enzyme than that calculated as being ordered from the electron cryomicroscopy. Henderson et al. (1977), using images of negatively stained 'crystals', selected by optical diffraction and processed by densitometry, showed dimers inserted across lipid bilayers of collapsed vesicles composed of two interlocking membranes. The area occupied by one oxidase complex was 50–60 nm^2. Three-dimensional analysis of another crystal form revealed monomers with somewhat distorted Y shapes, at least 12 nm in length (Fuller et al., 1979), containing two domains forming the arms of the Y with a centre-to-centre separation of 4.0 nm. As in our analysis, the cytoplasmic side of the complex comprised a single large 'C' domain extending 5.5 nm from the bilayer surface. Such previously studied semicrystalline dimers were roughly symmetrical (Henderson et al., 1977; Valpuesta et al., 1990). Shape analysis of the projecting protein in the present replicas has also given no indication of systematic asymmetries (results not shown). Reconstituted dimers maintain a symmetrical appearance (round or oval) with deviations possibly corresponding to conformational changes and/or tilting of the complex in the membrane. We are currently attempting to obtain a more precise shape distribution analysis using tantalum/tungsten shadowing which gives a higher resolution than does Pt/C with the freeze–fractured replicas.

Note added in proof (received 13 April 1993)

We also acknowledge important discussions with Dr. George C. Ruben, whose earlier work in this area (Ruben and Telford, 1980) should have been referenced.

This work was supported by NSERC (Canada) operating grant no. A-0412 to P.N. We thank Dr. Peter Rand for the use of the Balzers' freeze–fracture apparatus, Ms. Nola Fuller for assistance with freeze–fracturing and electron microscopy and Dr. Mohan S. Manocha for advice concerning the use of the Philips 300 electron microscope. We are grateful to Dr. John M. Wrigglesworth of King's College, London, U.K. and Dr. Peter Butko of NRC Ottawa for discussion and comments.

REFERENCES

Ames, B. N. (1966) Methods Enzymol. **8**, 115–118
Brunori, M., Antonini, G., Malatesta, F., Sarti, P. and Wilson, M. T. (1987) Eur. J. Biochem. **169**, 1–8
Capaldi, R., Malatesta, F. and Darley-Usmar, V. (1983) Biochim. Biophys. Acta **726**, 135–148
Capaldi, R., Takamiya, S., Zhang, Y., Gonzalez-Halphen, D. and Yanamura, W. (1987) Curr. Top. Bioenerg. **15**, 91–112
Casey, R., Ariano, B. and Azzi, A. (1982) Eur. J. Biochem. **122**, 313–318
Chen, P. S., Toribara, T. Y. and Warner, H. (1956) Anal. Chem. **28**, 1756–1758
Cooper, C. and Nicholls, P. (1990) Biochemistry **29**, 3865–3871
Cooper, C., Bruce, D. and Nicholls, P. (1990) Biochemistry **29**, 3859–3865
Cooper, C. E., Nicholls, P. and Freedman, J. A. (1991) Biochem. Cell. Biol. **69**, 586–607
Costello, M. and Frey, T. (1982) J. Mol. Biol. **162**, 131–156
Crinson, M. and Nicholls, P. (1992) Biochem. Cell. Biol. **70**, 301–308
Deatherage, J., Henderson, R. and Capaldi, R. (1982a) J. Mol. Biol. **158**, 487–499
Deatherage, J., Henderson, R. and Capaldi, R. (1982b) J. Mol. Biol. **158**, 501–514
Fajer, P. Knowles, P. and Marsh, D. (1989) Biochemistry **28**, 5634–5643
Falk, K. and Karlsson, B. (1979) FEBS Lett. **98**, 25–27
Folch, J., Lees, L. and Stanley, G. H. S. (1957) J. Biol. Chem. **226**, 497–509
Frey, T., Costello, M., Karlsson, B., Haselgrove, J. and Leigh, J. (1982) J. Mol. Biol. **162**, 113–130
Fuller, S., Capaldi, R. and Henderson, R. (1979) J. Mol. Biol. **134**, 305–327
Gregory, L. and Ferguson-Miller, S. (1989) Biochemistry **28**, 2655–2662
Henderson, R., Capaldi, R. and Leigh, J. (1977) J. Mol. Biol. **112**, 631–648
Hill, B. and Robinson, N. (1986) J. Biol. Chem. **261**, 15356–15359
Krab, K. and Wikström, M. (1978) Biochim. Biophys. Acta **504**, 200–214
Kuboyama, M., Yong, F. and King, T. (1972) J. Biol. Chem. **247**, 6375–6383
Longmuir, K., Capaldi, R. and Dahlquist, F. (1977) Biochemistry **16**, 5746–5755
Madden, T. and Cullis, P. (1984) J. Biol. Chem. **259**, 7655–7658
Madden, T., Hope, M. and Cullis, P. (1983) Biochemistry **22**, 1970–1974
Madden, T., Hope, M. and Cullis, P. (1984) Biochemistry **23**, 1413–1418
Moroney, P. M., Scholes, T. A. and Hinkle, P. C. (1984) Biochemistry **23**, 4991–4997
Nalecz, K., Bolli, R., Ludwig, B. and Azzi, A. (1985) Biochim. Biophys. Acta **808**, 259–272
Naqui, A., Kumar, C., Ching, Y. and Chance, B. (1984) Biochemistry **23**, 6222–6227
Nicholls, P. (1990) Biochem. Cell Biol. **68**, 1135–1141
Nicholls, P. and Hildebrandt, V. (1978) Biochem. J. **173**, 65–72
Nicholls, P. and Shaughnessy, S. (1985) Biochem. J. **228**, 201–210
Nicholls, P., Hildebrandt, V. and Wrigglesworth, J. M. (1980) Arch. Biochem. Biophys. **204**, 533–543
Nicholls, P., Cooper, C., Freedman, J. and Leece, B. (1988a) Biochem. Cell Biol. **66**, 1218–1225
Nicholls, P., Cooper, C. and Kjarsgaard, J. (1988b) in Advances in Membrane Biochemistry and Bioenergetics (Kim, C., Tedeschi, H., Diwan, J. and Salerno, J., eds.), pp. 311–321, Plenum Press, New York
Nicholls, P., Cooper, C. and Wrigglesworth, J. (1990) Biochem. Cell Biol. **68**, 1128–1134
Nicholls, P., Tattrie, B., Butko, P. and Tihova, M. (1992) Biochem. Soc. Trans. **20**, 115s
Papa, S., Capitanio, N. and de Nitto, E. (1987) Eur. J. Biochem. **164**, 507–516
Powell, G., Knowles, P. and Marsh, D. (1990) Biochemistry **29**, 5127–5132
Racker, E. (1972) J. Membr. Biol. **10**, 221–235
Rand, P., Kachar, B. and Reese, T. (1985) Biophys. J. **47**, 483–489
Rietveld, A., Kemenade, T., Hak, T., Verkleij, A. and deKruijff, B. (1987) Eur. J. Biochem. **164**, 137–140
Rigell, C., Saussure, C. and Freire, E. (1985) Biochemistry **24**, 5638–5646
Robinson, N. (1982) Biochemistry **21**, 184–188
Robinson, N. and Talbert, L. (1986) Biochemistry **25**, 2328–2335
Ruben, G. C. and Telford, J. N. (1980) J. Microsc. **118**, 191–216
Saraste, M. (1990) Q. Rev. Biophys. **23**, 331–366
Scotto, A. and Zakim, D. (1985) Biochemistry **24**, 4066–4075
Seki, S. and Oda, T. (1970) Arch. Biochem. Biophys. **138**, 122–134
Sjöstrand, F. S. (1990) in Deducing Function from Structure, Vol. 1, A Different View of Membranes, pp. 192–234, Academic Press, San Diego
Tihova, M., Tattrie, B. and Nicholls, P. (1991) 34th Annu. Meet. Can. Fed. Biol. Soc., Kingston, Ont., Canada, abstr. 081
Tihova, M., Tattrie, B. and Nicholls, P. (1992) Proc. 50th Annu. Meet. Electron Microsc. Soc. USA, Boston, MA
Valpuesta, J., Henderson, R. and Frey, T. (1990) J. Mol. Biol. **214**, 237–251
Vik, S. and Capaldi, R. (1977) Biochemistry **16**, 5755–5759
Wilson, K. and Prochaska, L. (1990) Arch. Biochem. Biophys. **282**, 413–420
Wrigglesworth, J. M. (1985) J. Inorg. Biochem. **23**, 311–316
Wrigglesworth, J. M. (1988) Mol. Asp. Med. **10**, 223–232
Wrigglesworth, J. M., Wooster, M. S., Elsden, J. and Danneel, H.-J. (1987) Biochem. J. **246**, 737–744
Wrigglesworth, J. M., Cooper, C., Sharpe, M. and Nicholls, P. (1990) Biochem. J. **270**, 109–118
Zhang, Y., Capaldi, R., Cullis, P. and Madden, T. (1985) Biochim. Biophys. Acta **808**, 209–211

Received 17 August 1992/10 December 1992; accepted 13 January 1993